

CIRCULARLY POLARIZED SPIDRON FRACTAL SLOT ANTENNA ARRAYS FOR BROADBAND SATELLITE COMMUNICATIONS IN KU-BAND

Son Trinh-Van, Han Byul Kim, Gina Kwon,
and Keum Cheol Hwang*

Division of Electronics and Electrical Engineering, Dongguk University-Seoul, 26, Pil-dong 3-ga, Chung-gu, Seoul 100-715, South Korea

Abstract—In this paper, a novel circularly polarized Spidron fractal slot antenna array developed for broadband satellite communication in the Ku-band is discussed. A Spidron fractal slot configuration was utilized as a single radiating element to achieve circularly polarized radiation. The effects of altering the feeding position on the resonance behavior and the radiative characteristics were assessed. As a consequence, the design was expanded from a single element to a 2×2 subarray and further to a 4×4 array in order to enhance the bandwidth performance of the antenna when integrated with a sequential feeding network. Two prototype arrays were fabricated and tested, and measurements revealed that the 2×2 subarray has a 10-dB reflection coefficient bandwidth between 10 and 14.28 GHz, 3 dB axial ratio bands between 10.15 and 11.15 GHz and between 11.75 and 13.92 GHz, and a maximum gain of 11.4 dB at 13 GHz. The results for the 4×4 array indicated that both the 10-dB reflection coefficient and 3 dB axial ratio bandwidths cover the entire operating frequency from 10 to 15 GHz in the Ku-band. The maximum gain for the 4×4 array was 15.63 dB at 12.6 GHz.

1. INTRODUCTION

Owing to their low profile, light weight, and the ease with which they can be integrated with active devices, microstrip antennas have become widely used over the past few decades [1–8]. Recently, circularly polarized (CP) microstrip antennas, in particular, have been attracting

Received 4 January 2013, Accepted 12 February 2013, Scheduled 18 February 2013

* Corresponding author: Keum Cheol Hwang (kchwang@dongguk.edu).

considerable attention for their usefulness in many applications such as for satellite communications [9] and in radio frequency identification (RFID) readers [10, 11]. Microstrip-fed CP antennas may be classified as either single-feed or dual-feed, based on the number of feeders they employ; single-feed antennas are preferred, as they eliminate the need for 90° hybrid couplers. Several designs for single-feed CP antennas have been described, such as a Koch fractal boundary CP microstrip antenna [12], a compact CP patch antenna loaded with a metamaterial [13], and a shorted CP patch antenna using a high-permittivity substrate [14]. However, all of the single-feed CP antennas described above usually have the disadvantage of featuring a very narrow 3 dB axial ratio (AR) bandwidth (typically 1–4%). To increase the bandwidth performance, square-slot antennas with multiple monopole elements [15] or a halberd-shaped feeder [16] were proposed; these allow for 3 dB AR bandwidths of 28.03% and 29.1%, respectively. A technique based on a chiral metamaterial structure was also applied to enhance the performance of the CP antenna [17]. In [18], a pair-element technique was employed for a 4×4 array of spiral-slot antennas to widen the impedance and AR bandwidths. However, the impedance and 3 dB AR bandwidths were only 8.5% and 8.9%, respectively.

In order to improve both the AR bandwidth and purity of the circular polarization, a technique for sequential rotation feeding involving the application of a physical rotation to the radiating element and an appropriate phase offset to element excitation was introduced [19]. Several 4×4 arrays incorporating sequential rotation feeding techniques have been developed [20–22]. A 4×4 sequentially rotated patch antenna array fed by a series feed with a 3 dB AR bandwidth of 12.4% and a 2 : 1 voltage standing-wave ratio bandwidth of 14.7% was reported in [20]. In [21], another 4×4 sequential rotation array of aperture antennas fed by a coplanar waveguide (CPW) was also proposed. This array exhibited an impedance bandwidth of 10.6% and a 3 dB AR bandwidth of 11%. In a recent study, a 4×4 array of sequentially rotated, stacked CP patches was presented for L-band applications [22]. By employing a sequential rotation feeding technique, an array consisting of sixteen square patches exhibited a broad impedance bandwidth of 25% and a 3 dB AR bandwidth of 10%.

In this paper, we propose a novel broadband CP antenna array utilizing Spidron fractal slots as radiating elements that are fed by parallel sequential networks. As discussed in Section 2, the single antenna element of the proposed array is comprehensively investigated in terms of its design considerations and operation principle. In our design, the radiating Spidron fractal slot is excited by a single

microstrip feeding line in order to achieve broadband CP radiation. Two types of antennas are fed by a sequentially rotated feeder: a 2×2 subarray and 4×4 array and these are then designed, fabricated, and tested, as discussed in Section 3. Section 4 describes the results from simulations and measurements of the parameters of the two arrays including the 10-dB reflection coefficient bandwidth, 3 dB AR bandwidth, and realized gain. Finally, concluding remarks are presented in Section 5.

2. SINGLE SPIDRON FRACTAL SLOT ANTENNA

2.1. Single Antenna Configuration

Figure 1 shows the configuration and design parameters for the single Spidron fractal slot antenna proposed in this paper (in an earlier study conducted by one of the present authors, another antenna design employing a Spidron fractal-shaped slot was proposed [23]). A Spidron fractal is a plane figure that is iteratively constructed from a series

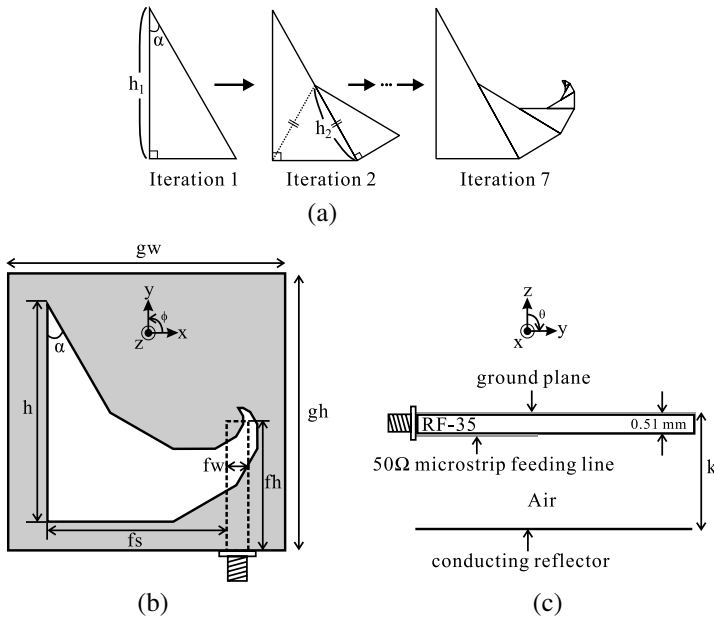


Figure 1. Configuration of a Spidron fractal slot antenna with a conducting reflector: (a) geometry of the Spidron fractal, (b) top view of the antenna, and (c) side view of the antenna.

of progressively smaller, contiguous right triangles using a common angular factor (α). From Fig. 1(a), it can be seen that the hypotenuse of each right triangle coincides with one of the legs of its succeeding, down-scaled triangle. It should be noted that α is one of the angles opposite the right angle in the first right triangle, while h is the length of the leg adjacent to angle α . The scaling factor (δ) is the ratio between the lengths of the sides of two successively generated right triangles and is determined by

$$\delta = \frac{h_{n+1}}{h_n} = \tan \alpha, \quad \text{for } 0^\circ < \alpha < 45^\circ. \quad (1)$$

As shown in Figs. 1(b) and 1(c), the proposed antenna element consists of a Spidron fractal slot etched from the ground plane, a microstrip feeding line printed onto the bottom of the dielectric substrate, and a conducting reflector located under the substrate. The antenna is fabricated on a Taconic RF-35 substrate having a thickness of 0.51 mm, dielectric constant of 3.5, and loss tangent of 0.0018. The Spidron fractal slot used in this design consists of seven iterated reductions of a right triangle. The 50- Ω microstrip feeding line located at an offset distance of f_s from one side of the Spidron fractal slot has a width and length of f_w and f_h , respectively. The overall dimensions of the single antenna are $g_w \times g_h \times k$ mm³, where k is the distance between the ground plane and the conducting reflector.

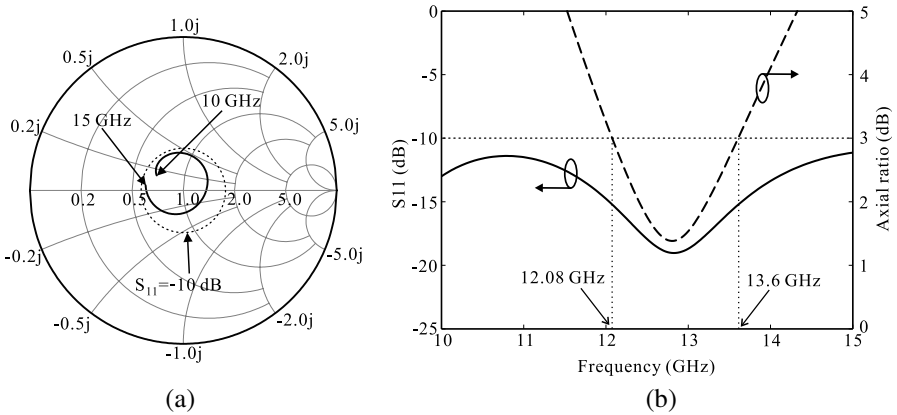


Figure 2. Simulated results for the single Spidron fractal slot antenna with optimized parameters of $h = 10$ mm, $\alpha = 30.1^\circ$, $k = 6$ mm, $f_s = 8.3$ mm, $f_w = 1$ mm, $f_h = 6$ mm, $g_w = 12.8$ mm, and $g_h = 12.8$ mm: (a) input impedance and (b) reflection coefficient and axial ratio.

2.2. Analysis of Single Antenna Element

The antenna was simulated using an ANSYS high-frequency structure simulation (HFSS) based on a three-dimensional finite element method (FEM). In the design process, several major parameters are examined: the leg length h , the angular factor α , the length of the microstrip feeding line fh , and the offset distance fs . The distance factor k was set to 6 mm, which is a quarter-wavelength ($\lambda_0/4$) of the radiation at a

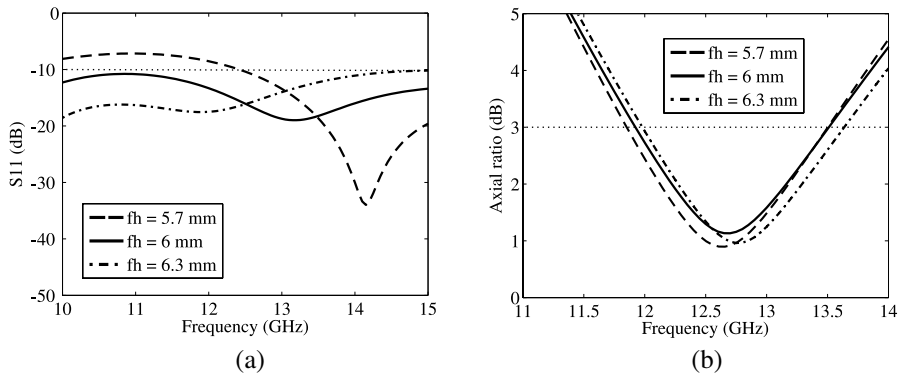


Figure 3. Simulated results for the single Spidron fractal slot antenna for various values of fh : (a) reflection coefficient and (b) axial ratio. Note that the other antenna parameters are given in the caption of the Figure 2.

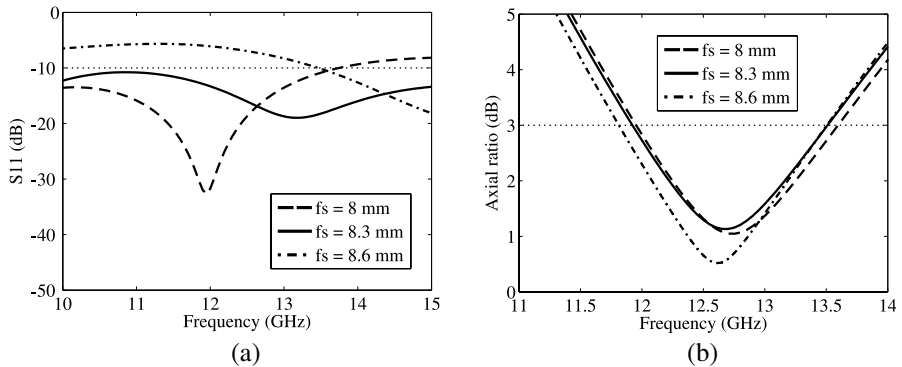


Figure 4. Simulated results for the single Spidron fractal slot antenna for various values of fs : (a) reflection coefficient and (b) axial ratio. Note that the other antenna parameters are given in the caption of the Figure 2.

frequency $f_0 = 12.5$ GHz, in order to obtain constructive interference along the positive z -axis direction. On the basis of parametric analyses, the optimized parameters for the proposed single Spidron fractal slot antenna are determined and summarized in the caption of the Fig. 2. Fig. 2 shows the simulated input impedance, reflection coefficient, and AR of the single Spidron fractal slot antenna using the optimized parameters. It can be seen that the input impedance is close to 50Ω with variations at 33 and 72Ω at 10.1 and 12.6 GHz, respectively, while the magnitude of the imaginary component varies from -11.6Ω at 13.55 GHz to 26.7Ω at 11.65 GHz. Therefore, the single antenna element exhibits a low reflection coefficient less than 10 -dB over the entire operating frequency band (10 to 15 GHz). An AR bandwidth less than 3 dB is also achieved between 12.08 and 13.6 GHz (11.8%).

Figure 3 shows the effects when varying the length of the feeding line fh on the reflection coefficient and AR performance. It is found that fh does not have much of an effect on the AR performance, although increasing fh shifts the resonant band to a lower frequency region. Fig. 4 illustrates the effects on the reflection coefficient and AR

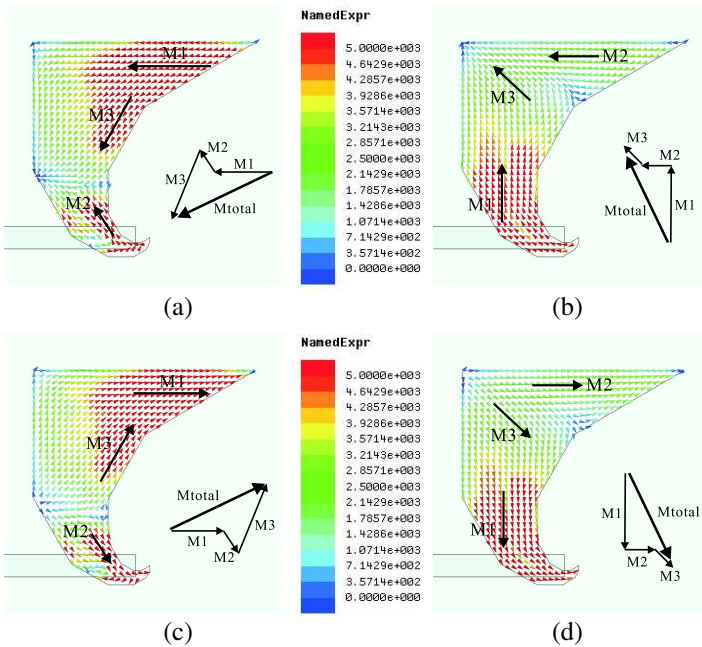


Figure 5. Simulated magnetic current distribution with a period T at 12.5 GHz: (a) $t = 0$, (b) $t = T/4$, (c) $t = 2T/4$, and (d) $t = 3T/4$.

performance arising from adjustments to the feeding position fs with h , fh , and α fixed at 10 mm, 6 mm, and 30.1° , respectively. Similar to the results shown in Fig. 3, a variation in fs changes the resonant frequency without significant deterioration in the AR performance.

In order to visualize the operation of the proposed antenna, the magnetic current concentrations of the aperture were simulated to investigate the generation of CP within the operating band. Fig. 5 illustrates the current distribution, which is observed from the positive z -direction at 12.5 GHz. Note that M_{total} represents the vector sum of all major current contributions. At $t = 0$, the currents on the first and second right triangles of the Spidron fractal slot rise and their vector sum points from the upper right corner to the lower left corner. At $t = T/4$, the currents on the Spidron fractal slot near the feeder dominate the radiation, producing a vector sum pointing from the lower right corner to the upper left corner. This vector sum is orthogonal to that at $t = 0$ and rotates clockwise as the time t increases, as shown in Fig. 5, thereby producing left-hand circular polarization (LHCP).

Figure 6 illustrates the simulated radiation patterns for a single Spidron fractal slot antenna having the optimized parameters. The unidirectional radiation pattern indicates a co-polarization (LHCP)

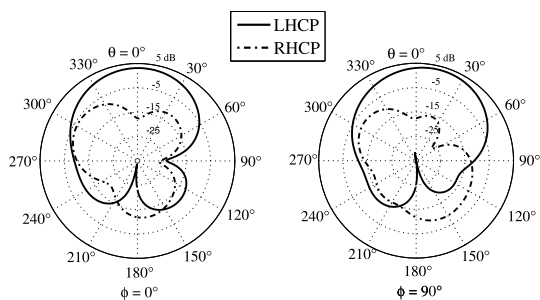


Figure 6. Simulated radiation patterns of a single antenna element at 12.5 GHz.

Table 1. Simulated gain of the single antenna element versus frequency.

Frequency (GHz)	11	11.5	12	12.5	13	13.5	14
LHCP gain (dB)	1.5	2.1	2.7	3.1	3.3	3.5	3.6
RHCP gain (dB)	-7.2	-8.8	-12	-17.5	-17.8	-12.9	-8.7

gain of 3.1 dB at 12.5 GHz in the broadside direction ($\theta = 0^\circ$). The cross-polarization (right-hand circular polarization, or RHCP) gain is -17.5 dB. The gains at other resonant frequencies are listed in Table 1. We note that backward radiation was successfully suppressed by the conducting reflector. As shown in Fig. 6, the main beam direction is slightly shifted away from the broadside direction because of the asymmetry in the Spidron fractal slot. However, this effect can be mitigated using the sequentially rotated array design described in the next section.

3. ANTENNA ARRAY AND FEEDING NETWORK

After the comprehensive assessment of the impedance matching and radiation characteristics of a single Spidron fractal slot antenna, our scope extended to the design of a sequentially rotated CP array in order to enhance both the antenna gain and AR bandwidth. In this section, configurations for a 2×2 subarray and 4×4 array that have both been integrated with parallel sequential feeding networks are presented in detail.

3.1. 2×2 Subarray Configuration

Figure 7 shows the configuration of a 2×2 subarray that utilizes the proposed Spidron fractal slots as its radiating element and a sequential

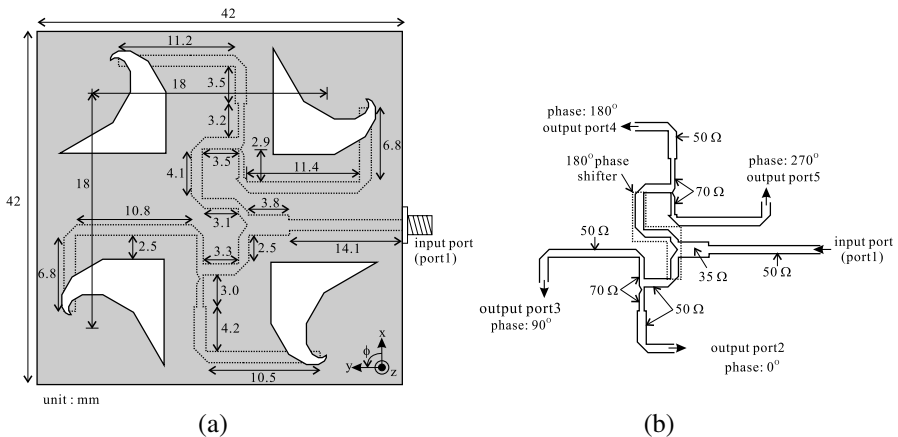


Figure 7. (a) Top view of the 2×2 subarray showing the detailed dimensions of the feeding network and (b) the parallel sequential feeding network.

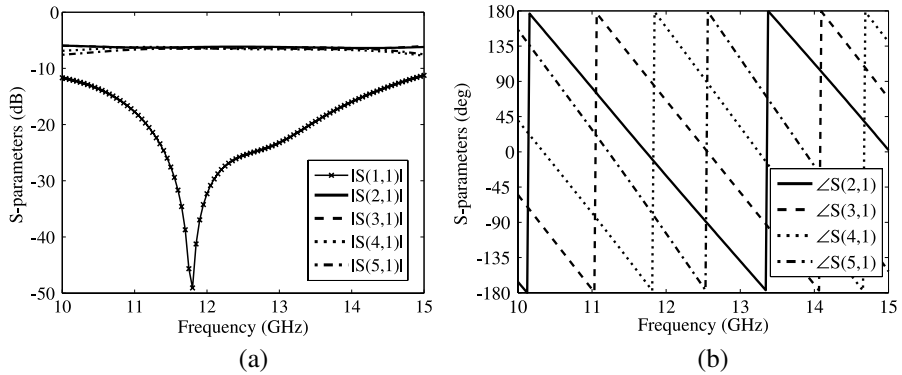


Figure 8. Simulated S -parameters of the sequential feeding network for the 2×2 subarray: (a) amplitudes and (b) phase distributions.

feeding network on a $42 \text{ mm} \times 42 \text{ mm}$ square substrate. The distance between each of the Spidron fractal slots along both the x - and y -axes is 18 mm , corresponding to $0.75\lambda_0$ at 12.5 GHz ; detailed dimensions are given in Fig. 7(a). In order to achieve LHCP operation, the fractal slots are sequentially rotated clockwise by 90° . The feeding network here is designed to excite each slot in turn with sequential phase delays of 90° . To implement this network design, three T-junction dividers and impedance transformers are used to match the impedances between $50\text{-}\Omega$ input port and four $50\text{-}\Omega$ output ports, as shown in Fig. 7(b). The center section of the feeding network is an equal power divider with a 180° phase difference. Each divided, anti-phased port is then connected to another T-junction divider in order to generate signals with 90° phase difference in two sets of output ports. Thus, the entire network consists of four output ports, each successively phase delayed by 90° in the clockwise direction. We note that the mitered sections on each T-junction power divider are slightly deviated from the center of the input microstrip line in order to optimize the amplitude balance of the network.

The simulated amplitude balance and phase distribution in the feeding network are shown in Fig. 8. Between 10 and 15 GHz , the reflection coefficient of the network is below 12-dB , while an amplitude deviation and phase error of less than 0.2 dB and 10° , respectively, are achieved at the central frequency of 12.5 GHz . The worst imbalance in power is observed between ports 2 and 5 at 10 GHz with an amplitude difference of 1.6 dB . At this frequency, the phase difference between these two ports was nearly 322° , i.e., 52° larger than the optimal value of 270° .

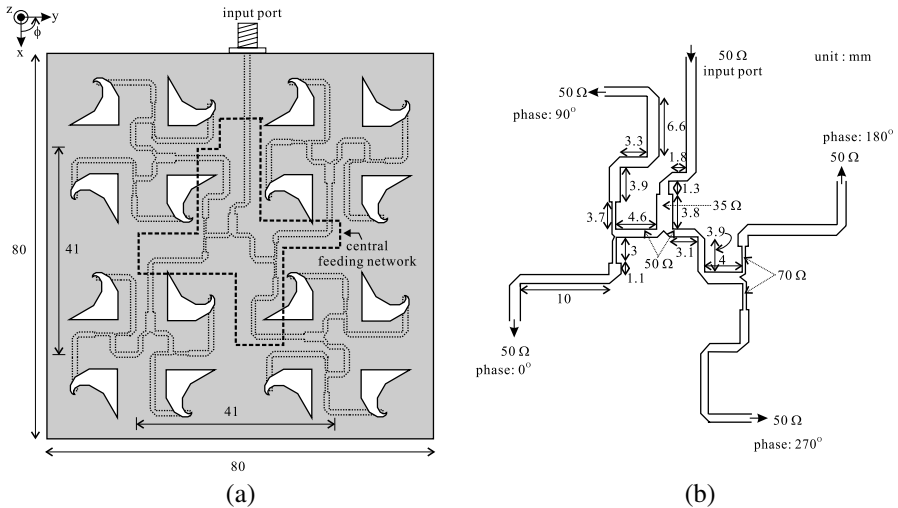


Figure 9. (a) Top view of the 4×4 antenna array and (b) detailed dimensions of the central sequential feeding network.

3.2. 4×4 Array Configuration

A high-gain, CP 4×4 array developed for broadband satellite communication in the Ku-band is described in this sub-section. Fig. 9(a) shows the geometry of the 4×4 array that incorporates four 2×2 subarrays as individual radiating elements. The subarrays are arranged in a 2×2 configuration on a square substrate having overall dimensions of $80 \text{ mm} \times 80 \text{ mm}$ and a center-to-center distance of 41 mm between the subarrays along both the x - and y -axes. To service the four sequentially rotated 2×2 subarrays, an additional sequential feeding network is utilized. For this, each subarray input is connected to one output port of the central sequential feeding network, as shown in detail in Fig. 9(b). The central sequential feeding network is designed using the same procedure used for the 2×2 subarray feeding network shown in Fig. 7(b).

4. FABRICATION AND MEASUREMENT

Figure 10 shows photographs of a 2×2 subarray and 4×4 array. Both are fabricated on Taconic RF-35 substrates having a thickness of 0.51 mm. Four Teflon supports are used to support the substrate that is suspended in midair above the conducting reflector. Fig. 11(a) shows the simulated and measured reflection coefficients of the 2×2 subarray.

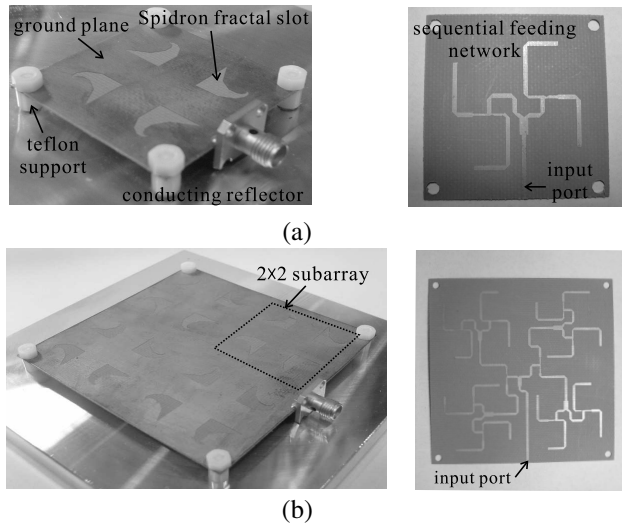


Figure 10. Photographs of the fabricated antennas: (a) 2×2 subarray and (b) 4×4 array.

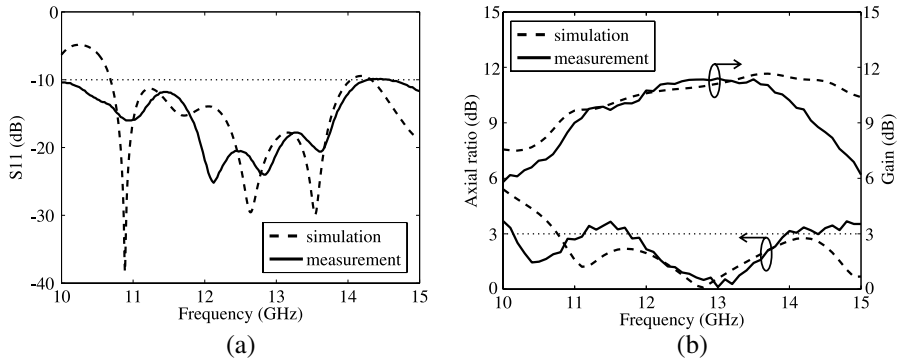


Figure 11. Simulated and measured results of the 2×2 subarray versus frequency: (a) reflection coefficients and (b) axial ratios and gains.

The measured reflection coefficient is lower than -10-dB between 10 and 14.28 GHz, whereas the simulated 10-dB reflection bandwidth ranges from 10.69 to 14.04 GHz. The simulated and measured results for the AR of the 2×2 subarray are shown in Fig. 11(b). A 3 dB AR bandwidth ranging from 10.75 to 15 GHz is obtained from the simulation, while the measured results feature two 3 dB AR bandwidths ranging from 10.15

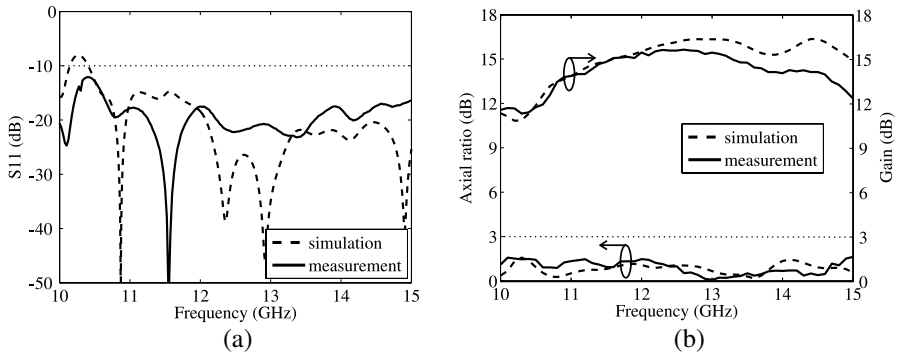


Figure 12. Simulated and measured results of the 4×4 array versus frequency: (a) reflection coefficients and (b) axial ratios and gains.

to 11.15 GHz and from 11.75 to 13.92 GHz. The small discrepancy between the simulation and the measurement is attributed to the tolerances in the fabrication and measurement. Fig. 11(b) also shows the realized gain for co-polarized (LHCP) radiation against the frequency at the broadside. The simulated peak gain ranges from 7.5 dB at 10.2 GHz to 11.7 dB at 13.7 GHz, whereas the measured gain varies from 5.8 dB at 10 GHz to 11.4 dB at 13 GHz. It is worth noting that the performance of the 2×2 subarray prototype (3 dB AR bandwidth and gain) is significantly better than that of the single Spidron fractal slot antenna discussed in Section 2.

Figure 12(a) shows the simulated and measured reflection coefficients of the 4×4 array configuration. The simulated 10-dB reflection bandwidth ranges from 10.4 to 15 GHz, while the measured 10-dB reflection bandwidth covers the entire frequency range. The simulated and measured results for the AR and gain are shown in Fig. 12(b); overall, they agree well with each other. We find that the CP performance is further enhanced by applying sequential rotation feeding into the four 2×2 subarrays, as both the simulated and measured ARs are lower than 1.5 dB over the entire measured frequency range. The measured broadside gain varies from 11.31 dB at 10.3 GHz to 15.63 dB at 12.6 GHz. Table 2 shows a comparison of the proposed 4×4 array antenna and the antennas presented in earlier works [18, 20–22] in terms of the reflection and 3 dB AR bandwidths. The proposed 4×4 array utilizing a Spidron fractal slot has broader bandwidth compared to the previous 4×4 arrays.

The measured CP radiation patterns along two elevation cuts (xz - and yz -planes) of the fabricated 2×2 subarray and 4×4 array are illustrated in Fig. 13. The experimental results for the 2×2 subarray

Table 2. Comparison of the AR and reflection bandwidths between the proposed 4×4 array and 4×4 arrays in other studies.

Structure	Description	3 dB AR bandwidth	10-dB reflection bandwidth
Proposed array	Spidron fractal slot array	10–15 GHz (40%)	10–15 GHz (40%)
[18]	Spiral slot array	11.32–12.38 GHz (8.9%)	11.35–12.35 GHz (8.5%)
[20]	Dual-fed patch array	5.44–6.16 GHz (12.4%)	5.38–6.23 GHz (14.7%)
[21]	CPW-fed aperture array	23.8–26.52 GHz (11%)	23.85–26.51 GHz (10.6%)
[22]	Stacked patch array	1.52–1.67 GHz (10%)	1.4–1.8 GHz (25%)

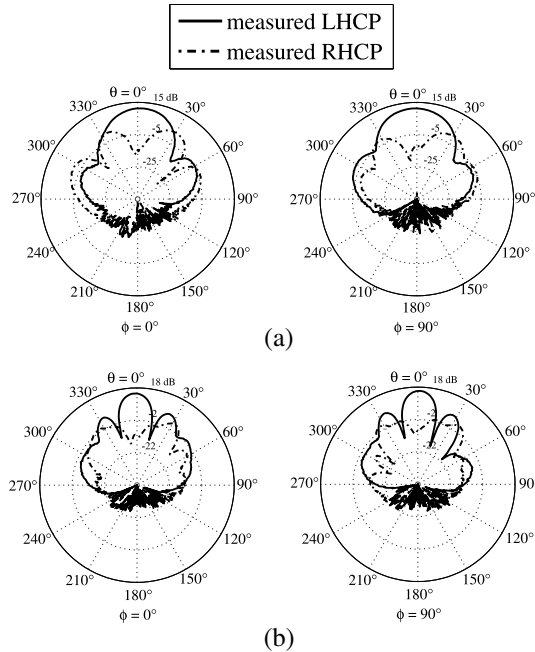


Figure 13. Measured radiation patterns of the fabricated arrays at 12.5 GHz: (a) 2×2 subarray and (b) 4×4 array.

show a cross-polarization (RHCP) suppression level larger than 23.5 dB in the broadside direction, while a front-to-back ratio higher than 36.8 dB is achieved at 12.5 GHz. The 4×4 array antenna also attains a high cross-polarization suppression level of approximately 25.8 dB as well as a front-to-back ratio higher than 40.5 dB.

5. CONCLUSION

In this paper, a novel broadband CP fractal slot array was presented. The proposed array antenna utilized Spidron fractal slots and a parallel sequential feeding network to obtain circular polarization over a broad frequency range. Two prototypes, a 2×2 subarray and 4×4 array, were fabricated and tested to demonstrate performance characteristics. The experimental results showed that both array prototypes achieved broadband reflection and AR bandwidths spanning the entire operating frequency range of 10–15 GHz. In addition, the 4×4 array exhibited a maximum broadside gain of 15.63 dB. Therefore, array antennas using these configurations can be feasibly employed for broadband satellite communication within the Ku-band.

ACKNOWLEDGMENT

This work was supported by Basic Science Research Program through the National Research Foundation of Korea (NRF) funded by the Ministry of Education, Science and Technology (2012-0003052).

REFERENCES

1. Pozar, D. M., "Microstrip antennas," *Proc. IEEE*, Vol. 80, No. 1, 79–91, 1992.
2. Moradi, K. and S. Nikmehr, "A dual-band dual-polarized microstrip array antenna for base stations," *Progress In Electromagnetics Research*, Vol. 123, 527–541, 2012.
3. Gujral, M., J. L.-W. Li, T. Yuan, and C.-W. Qiu, "Bandwidth improvement of microstrip antenna array using dummy EBG pattern on feedline," *Progress In Electromagnetics Research*, Vol. 127, 79–92, 2012.
4. Wei, K. P., Z. J. Zhang, and Z. H. Feng, "Design of a dualband omnidirectional planar microstrip antenna array," *Progress In Electromagnetics Research*, Vol. 126, 101–120, 2012.
5. Monavar, F. M. and N. Komjani, "Bandwidth enhancement of microstrip patch antenna using Jerusalem cross-shaped frequency

- selective surfaces by invasive weed optimization approach,” *Progress In Electromagnetics Research*, Vol. 121, 103–120, 2011.
6. Asimakis, N. P., I. S. Karanasiou, and N. K. Uzunoglu, “Non-invasive microwave radiometric system for intracranial applications: A study using the conformal L-notch microstrip patch antenna,” *Progress In Electromagnetics Research*, Vol. 117, 83–101, 2011.
 7. Wang, X., M. Zhang, and S.-J. Wang, “Practicability analysis and application of PBG structures on cylindrical conformal microstrip antenna and array,” *Progress In Electromagnetics Research*, Vol. 115, 495–507, 2011.
 8. Tiang, J. J., M. T. Islam, N. Misran, and J. S. Mandeep, “Circular microstrip slot antenna for dual-frequency RFID application,” *Progress In Electromagnetics Research*, Vol. 120, 499–512, 2011.
 9. Garcia-Aguilar, A., J.-M. Inclan-Alonso, L. Vigil-Herrero, J.-M. Fernandez-Gonzalez, and M. Sierra-Perez, “Low-profile dual circularly polarized antenna array for satellite communications in the X band,” *IEEE Trans. Antennas Propag.*, Vol. 60, No. 5, 2276–2284, 2012.
 10. Lau, P.-Y., K. K.-O. Yung, and E. K.-N. Yung, “A low-cost printed CP patch antenna for RFID smart bookshelf in library,” *IEEE Trans. Ind. Electron.*, Vol. 57, No. 5, 1583–1589, 2010.
 11. Wang, P., G. Wen, J. Li, Y. Huang, L. Yang, and Q. Zhang, “Wideband circularly polarized UHF RFID reader antenna with high gain and wide axial ratio beamwidths,” *Progress In Electromagnetics Research*, Vol. 129, 365–385, 2012.
 12. Rao, P. N. and N. V. S. N. Sarma, “Fractal boundary circularly polarised single feed microstrip antenna,” *Electron. Lett.*, Vol. 44, No. 12, 713–714, 2008.
 13. Dong, Y., H. Toyao, and T. Itoh, “Compact circularly-polarized patch antenna loaded with metamaterial structures,” *IEEE Trans. Antennas Propag.*, Vol. 59, No. 11, 4329–4333, 2011.
 14. Tang, X., H. Wong, Y. Long, Q. Xue, and K. L. Lau, “Circularly polarized shorted patch antenna on high permittivity substrate with wideband,” *IEEE Trans. Antennas Propag.*, Vol. 60, No. 3, 1588–1592, 2012.
 15. Rezaeieh, S. A. and M. Kartal, “A new triple band circularly polarized square slot antenna design with crooked T and F-shape strips for wireless applications,” *Progress In Electromagnetics Research*, Vol. 121, 1–18, 2011.
 16. Sze, J.-Y. and S.-P. Pan, “Design of broadband circularly

- polarized square slot antenna with a compact size,” *Progress In Electromagnetics Research*, Vol. 120, 513–533, 2011.
17. Zarifi, D., H. Oraizi, and M. Soleimani, “Improved performance of circularly polarized antenna using semi-planar chiral metamaterial covers,” *Progress In Electromagnetics Research*, Vol. 123, 337–354, 2012.
 18. Nakano, H., K. Nakayama, H. Mimaki, J. Yamauchi, and K. Hirose, “Single-arm spiral slot antenna fed by a triplate transmission line,” *Electron. Lett.*, Vol. 28, No. 22, 2088–2090, 1992.
 19. Hall, P. S., “Application of sequential feeding to wide bandwidth, circularly polarised microstrip patch arrays,” *Proc. Inst. Elect. Eng. Microw., Antennas Propag.*, Vol. 136, No. 5, 390–398, 1989.
 20. Evans, H., P. Gale, and A. Sambell, “Performance of 4×4 sequentially rotated patch antenna array using series feed,” *Electron. Lett.*, Vol. 39, No. 6, 493–494, 2003.
 21. Soliman, E. A., S. Brebels, E. Beyne, and G. A. E. Vandenbosch, “Sequential-rotation arrays of circularly polarized aperture antennas in the MCM-D technology,” *Microw. Opt. Technol. Lett.*, Vol. 44, No. 6, 581–585, 2005.
 22. Kaffash, S. and M. Kamyab, “A sequentially rotated RHCP stacked patch antenna array for INMARSAT-M land applications,” *Proc. 6th European Conf. Antennas Propag. (EUCAP)*, 1–4, Prague, Czech Republic, 2012.
 23. Hwang, K. C., “Broadband circularly-polarised Spidron fractal slot antenna,” *Electron. Lett.*, Vol. 45, No. 1, 3–4, 2009.